Elucidating the Phase Transformation of $Li_4Ti_5O_{12}$ Lithiation at the Nanoscale

Michael G. Verde[1*], Loïc Baggetto[2], Nina Balke[3], Gabriel M. Veith[2], Joon Kyo Seo[4], Ziying Wang[1], Ying Shirley Meng[1*]

[1] Department of NanoEngineering, University of California San Diego, La Jolla, CA 92093, USA

[2] Materials Science and Technology Division, Oak Ridge National Lab, Oak Ridge, TN 37831, USA

[3] The Center for Nanophase Materials Sciences, Oak Ridge National Lab, Oak Ridge, TN 37831, USA

[4] Materials Science & Engineering Program, University of California San Diego, La Jolla, CA 92093, USA

*Corresponding Authors. (M.G.V) mverdejr@gmail.com; (Y.S.M) shmeng@ucsd.edu

Due to the demand for high energy density batteries for mobile electronics and electric vehicles, the quest for high capacity, low voltage anode materials – especially involving Si – has been heavily pursued in recent years. In this respect, $Li_4Ti_5O_{12}$ (LTO) is viewed as an inferior lithium ion battery anode. It exhibits relatively low capacity and high voltage compared to the most commercially available Li-ion anode, graphite (175 vs 372 $mAh \cdot g^{-1}$ and 1.55 vs ~ 0.1 V Li/Li^+). Nevertheless, the same undesirable properties that contribute to low energy densities provide attractive advantages as well. For example, the high redox potential of LTO lies safely within the electrolyte stability window.[1] This enables cycling without the formation of deleterious passivation layers, which are a problem for the long-term stability of conventional graphite anode and the popular alternatives such as silicon.[2] The two-phase reaction, which leads to moderate capacity, is also highly facile. It proceeds between two members ($Li_4Ti_5O_{12}$ and $Li_7Ti_5O_{12}$) that possess the same crystallographic space group, $Fd\bar{3}m$. Even upon intercalation of 3 Li^+ per formula unit, there is only a 0.2% volume change of the spinel lattice, resulting in its description as a *zero-strain* material.[3] The stability, robustness, and safety of LTO have in fact led to its successful commercialization.

While the ionic conductivity of LTO is comparable to other Li-ion anodes, a major shortcoming is its inherently low electronic conductivity.[4] $Li_4Ti_5O_{12}$ is considered to be an insulator, with experimentally reported band gaps typically between 3.0 and 4.0 eV. In order to circumvent this problem for use as an electrode, several strategies have been implemented. Coatings, such as carbon, have been applied to improve the electronic conductivity.[5] Doping with a host of cations has also been performed to decrease the band gap and improve performance.[6] Alternatively, LTO nanostructures have been synthesized to shorten Li^+ diffusion lengths and increase surface areas.[7] By applying these treatments, extremely high reversible rates of up to 100C (full charge or discharge in almost 30 seconds) have been reported.[8] Understanding exactly how the phase transformation between $Li_4Ti_5O_{12}$ and $Li_7Ti_5O_{12}$ proceeds and what factors promote, however, is still relatively ill-defined. Because the lattice parameters of both structures are near identical, few diffraction techniques are able to physically differentiate them.

This work exploits the most significant property difference between the two phases – their difference in electronic conductivity – in order to more fully explain the insulator-metal transition occurring within the system. Using conductive atomic force microscopy (c-

AFM) we directly visualize the formation and distribution of each phase at the nanoscale, for the first time (*Figure 1*). We present comprehensive current and topography maps of LTO, at various states of charge, to demonstrate where the transition between these two phases occurs, and what features promote it. These results are combined with chemistry-resolved surface measurements using X-ray photoelectron spectroscopy (XPS), at the same states of charge, to explain changes in surface morphology and composition. The unique application of the SPM methods presented here is a valuable key for the future optimization of this material, its composite electrode, and others like it.

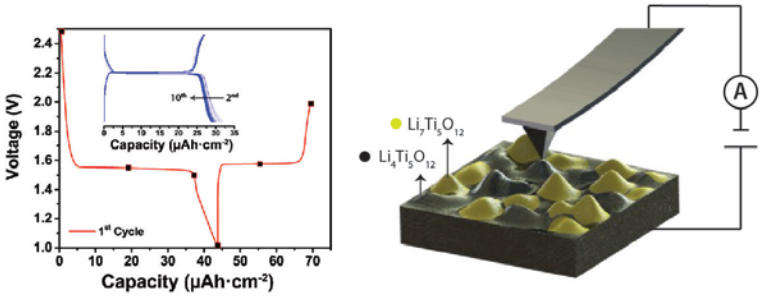

Figure 1. First cycle electrochemical profile of thin-film Li4Ti5O12 anode vs Li/Li$^+$, with squares indicating points where samples were characterized, and first 10 cycles – inset (left). An illustration of the c-AFM capability to detect the presence of each phase due to their unique conductivities (right).

LTO electrochemistry

In order to determine how LTO's fundamental mechanism proceeds, we made use of thin-films that possessed only the electrochemically active material. LTO was grown on Pt-coated (*ca*. 225 nm) Al_2O_3 disks using RF magnetron sputtering and exhibit a thickness around 800 nm. The Pt layer was incorporated to ensure good electrical contact for use in batteries as well as for c-AFM analysis. *Figure 1* highlights the material's first electrochemical cycle and demonstrates very good reversibility over the first 10 cycles. The flat redox potential at 1.55 V vs Li/Li$^+$ is clearly indicative of the two-phase reaction between $Li_4Ti_5O_{12}$ and $Li_7Ti_5O_{12}$, as has been previously reported.[9] In order to explore the unique changes occurring in this system during the first cycle, we analyze the thin-films at the points indicated along the voltage profile in *Figure 1*: 1) pristine LTO; 2) LTO discharged to 50% of the initial discharge capacity; 3) LTO immediately following the voltage plateau, discharged to 1.5 V; 4) LTO fully discharged to 1.0 V; 5) LTO charged to 50% of the 1st charge capacity; 6) LTO fully charged to 2.0 V.

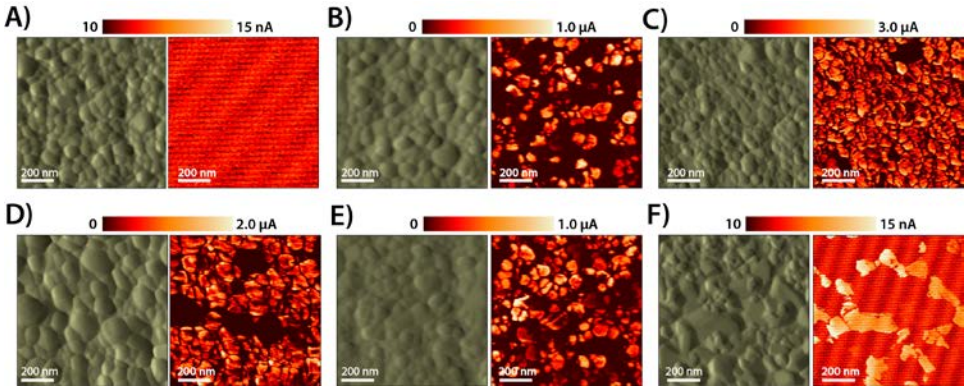

Figure 2. AFM deflection (left) and current (right) images of LTO thin-films cycled to various states of charge, corresponding to (A) pristine, (B) discharged 50%, (C) discharged to 1.5V, (D) discharged to 1.0V, (E) charged 50%, and (F) charged to 2.0V. Note the difference in units between scale bars.

LTO conductivity

While the morphology did not change upon initial discharge, due to negligible volume expansion upon lithiation, the electronic conductivity measured using c-AFM significantly increased. *Figure 2* depicts the current response of all samples when a potential of 0.4 V was applied between the c-AFM tip and substrate. While no current is observed in the pristine material, it is measured within an array of individual grains upon discharging to 50% capacity. *Figure 2b* suggests that the transition of $Li_4Ti_5O_{12}$ to $Li_7Ti_5O_{12}$ proceeds *via* a limited number of narrow percolation channels that connect current collector and electrolyte. *Figure 2c* demonstrates that immediately following the total lithiation, or completion of the two-phase reaction, nearly all grains in the LTO film are electronically conductive.

In order to summarize and compare the wide range of measured currents (from nA to □A), the log(current) values of all samples are shown in *Figure 3*. Current histograms of the measured c-AFM images are depicted in *Figure 3a*. On the left is the low current region, with the single peak corresponding to noise at the instrument's detection limit. On the right is the high current region, resulting from current measured because of changes among each sample. As the LTO sample is discharged, its measured current increases, which results in the low current peak decreasing and the high current peak increasing, until it reaches its maximum when discharged to 1.5 V. Further discharge to 1.0 V reduces the current and the area fraction of regions showing current, with a strong increase in surface roughness (*Figures 3b & 3c*). Upon charge, the average current and surface roughness decrease again. While the average current of samples discharged and charged to 50% were fairly similar, their RMS surface roughnesses were not. The difference in morphology is likely related to the first cycle partial irreversibility, where surface reconstruction occurred below 1.5 V of the initial discharge.

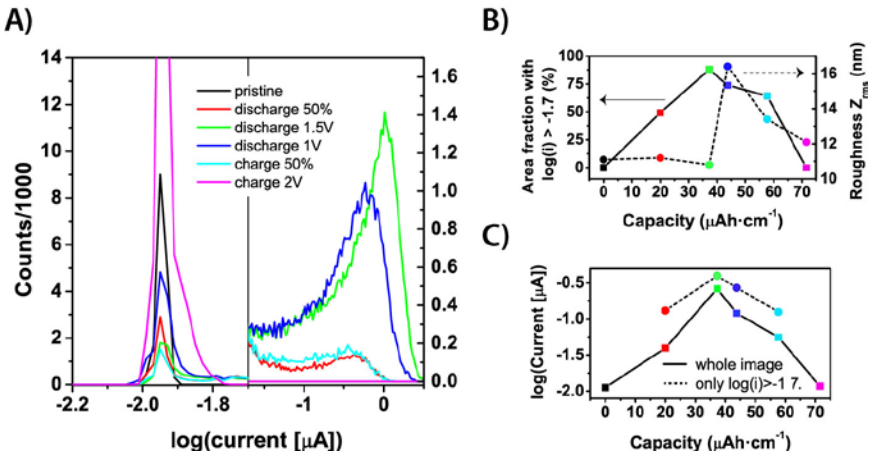

Figure. 3 (A) Histograms of c-AFM images for all samples divided in two regimes. (B) Area fraction of regions where current is measured (left axis), as well as surface roughness (right axis), as a function of the first cycle capacity. Note that discharge to 1.5 V and 1.0 V corresponds to 37μA·cm^2 and 44 μA·cm^2, respectively. Larger capacities correspond to the first charge. (C) Average current measured in the whole images of Figure 2 and average current measured in areas exhibiting current above a certain threshold.

LTO surface chemistry

To further understand the LTO phase transition and the evolution of surface chemistry during the first cycle, we performed XPS on thin-films cycled to the same states of charge described previously. *Figure 4* shows high-resolution scans of the C1s, O1s, and Ti2p regions. The single peak centered at 458.0 eV corresponds very well to the $2p_{3/2}$ peak of Ti^{4+} in LTO, as well as in TiO_2.[10] Upon discharge, a second peak at 455.9 eV forms, which corresponds to Ti^{3+} measured in Ti_2O_3. This peak reaches a maximum relative to the Ti^{4+} peak, in the LTO sample discharged to 1.0 V and correlates to the formation of Ti^{3+} due to reduction of Ti^{4+} upon lithiation. The relative intensity of the Ti^{3+} peak decreases upon charge and completely disappears at 2.0 V, indicating that the surface reaction is fully reversible.

The peak in the O1s spectra at 529.7 eV corresponds to O^{2-} in the LTO lattice. Upon discharge, a peak at 531.5 eV grows relative to it, and reaches a maximum at 1.0 V. This higher binding energy peak results from the contributions of several solid electrolyte interface (SEI) species, including CO_3^{2-}, -CO_2- and $Li_xPO_xF_z$, all of which originate from the decomposition of electrolyte.[11] The formation of decomposition products, Li_2CO_3 and/or $LiCO_3R$, are also shown to significantly occur in the sample discharged to 1.0 V, as suggested by the signal in the C1s peak near 289.5 eV.[12] The fact that we observe these species is significant because LTO is excessively championed to form no passivation or SEI layers, due to its high redox potential. This is clearly not the case. A passivation layer may form upon initial discharge (below 1.5 V) to create a relatively stable SEI; since subsequent cycles show markedly improved capacity retention, this reduction of electrolyte would not appear to occur continuously.

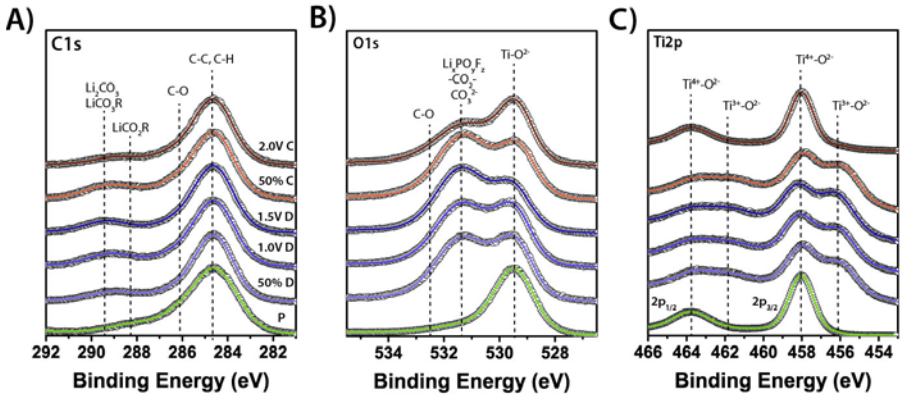

Figure 4. Normalized high-resolution C1s (A), O1s (B), and Ti2p (C) XPS spectra of the LTO thin-films discharged (blue) and then charged (red). From bottom to top is pristine (P), discharged 50% (50% D), discharged to 1.5V (1.5V D), discharged to 1.0V (1.0V D), charged 50% (50% C), and charged to 2.0V (2.0V C).

The combination of c-AFM and XPS described provides a more detailed understanding of the LTO lithiation/delithiation process. These insights may be used to optimize other materials with insulator to metal transitions behaviors. More detail regarding these results can be found in the following publication: Verde, M. G. et al. *ACS Nano* **2016,** *10* (4), 4312-4321.

This work has been a collaborative effort between UCSD and Oak Ridge National Lab and was supported by the U.S. Department of Energy, Office of Basic Energy Sciences, under Award Number DE-FG02-10ER46672 (DE-SC0002357).

References

1. Goodenough, J. B.; Kim, Y. Challenges for Rechargeable Li Batteries. *Chem. Mater.* **2009,** *22* (3), 587-603.
2. Oumellal, Y.; Delpuech, N.; Mazouzi, D.; Dupre, N.; Gaubicher, J.; Moreau, P.; Soudan, P.; Lestriez, B.; Guyomard, D. The failure mechanism of nano-sized Si-based negative electrodes for lithium ion batteries. *J. Mater. Chem.* **2011,** *21* (17), 6201-6208.
3. Ohzuku, T.; Ueda, A.; Yamamoto, N. Zero-Strain Insertion Material of Li[Li1/3Ti5/3]O4 for Rechargeable Lithium Cells. *J. Electrochem. Soc.* **1995,** *142* (5), 1431-1435.
4. Takami, N.; Hoshina, K.; Inagaki, H. Lithium Diffusion in Li4/3Ti5/3O4 Particles during Insertion and Extraction. *J. Electrochem. Soc*. **2011,** *158* (6), A725-A730.
5. Luo, H.; Shen, L.; Rui, K.; Li, H.; Zhang, X. Carbon coated Li4Ti5O12 nanorods as superior anode material for high rate lithium ion batteries. *J. Alloys Compd.* **2013,** *572* (0), 37-42.
6. Zhang, Q.; Verde, M. G.; Seo, J. K.; Li, X.; Meng, Y. S. Structural and electrochemical properties of Gd-doped Li4Ti5O12 as anode material with improved rate capability for lithium-ion batteries. *J. Power Sources* **2015,** *280* (0), 355-362.
7. Chen, S.; Xin, Y.; Zhou, Y.; Ma, Y.; Zhou, H.; Qi, L. Self-supported Li4Ti5O12 nanosheet arrays for lithium ion batteries with excellent rate capability and ultralong cycle life. *Energy Environ. Sci.* **2013**.
8. Liu, J.; Song, K.; van Aken, P. A.; Maier, J.; Yu, Y. Self-Supported Li4Ti5O12-C Nanotube Arrays as High-Rate and Long-Life Anode Materials for Flexible Li-Ion Batteries. *Nano Lett.* **2014,** *14* (5), 2597-2603.
9. Li, D.; Zhou, H. Two-phase transition of Li-intercalation compounds in Li-ion batteries. *Materials Today* **2014,** *17* (9), 451-463.
10. Cai, R.; Jiang, S.; Yu, X.; Zhao, B.; Wang, H.; Shao, Z. A novel method to enhance rate performance of an Al-doped Li4Ti5O12 electrode by post-synthesis treatment in liquid formaldehyde at room temperature. *J. Mater. Chem.* **2012,** *22* (16), 8013-8021.
11. Baggetto, L.; Dudney, N. J.; Veith, G. M. Surface chemistry of metal oxide coated lithium manganese nickel oxide thin film cathodes studied by XPS. *Electrochim. Acta* **2013,** *90*, 135-147.
12. Appapillai, A. T.; Mansour, A. N.; Cho, J.; Shao-Horn, Y. Microstructure of LiCoO2 with and without "AlPO4" Nanoparticle Coating: Combined STEM and XPS Studies. *Chem. Mater.* **2007,** *19* (23), 5748-5757.